

Petrogenesis and Tectonic Implications of the Paiku Leucogranites, Northern Himalaya

Zhengbin Gou¹, Xin Dong^{1*}, Baodi Wang¹

1. Chengdu Center, China Geological Survey, Chengdu 610081, China

2. Key Laboratory of Deep-Earth Dynamics of Ministry of Natural Resources, Institute of Geology, Chinese Academy of Geological Sciences, Beijing 100037, China

¹Zhengbin Gou: <https://orcid.org/0000-0002-0975-3557>; ¹Xin Dong: <https://orcid.org/0000-0002-8649-7104>

ABSTRACT: The Himalayan leucogranites provide insights into the partial melting behavior of relatively deeper crustal rocks and tectono-magmatic history of the Himalayan Orogen. The Paiku leucogranites of northern Himalaya can be subdivided into two-mica leucogranite (TML), garnet-bearing leucogranite (GL), cordierite-bearing leucogranite (CL), and tourmaline-bearing leucogranite (TL). All of them are high-K, peraluminous, calc-alkalic to alkali-calcic rocks. They are enriched in light rare earth elements (LREE) and large ion lithophile elements (LILE), and show pronounced negative anomalies of Sr, Ba, K and Ti, but positive anomalies of Nb and Rb. LA-ICP-MS U-Pb zircon dating of one TML, one GL, and two CL samples yielded variable $^{206}\text{Pb}/^{238}\text{U}$ ages ranging from 23.6 to 16.1 Ma, indicating the Paiku leucogranites underwent a low degree of partial melting process. Combining with previous studies, we suggest the Paiku leucogranites were derived from partial melting of metasedimentary rocks of the Higher Himalayan Sequence (HHS). The GL and TL mainly resulted from the muscovite-dehydration melting, whereas the TML and CL were mainly derived from the biotite-dehydration melting. Finally, it is concluded that the Paiku leucogranites were probably formed during the subduction of the Indian crust.

KEY WORDS: Paiku leucogranites, petrochemistry, U-Pb geochronology, dehydration melting, tectonic implications, northern Himalaya.

0 INTRODUCTION

The Himalayan Orogen, the youngest and largest ongoing continent-continent collisional orogen on the Earth (Yin, 2006), experienced multistage high-grade metamorphism and progressive partial melting, which resulted in the formation of various types of granites and leucogranites (King et al., 2011; Patino Douce and Harris, 1998). Understanding emplacement timing and geochemical feature of these leucogranites in the Himalaya provides insight into the melting behaviors of crustal rocks during collisional orogenic processes and tectonic evolution of the orogen (Liu et al., 2014; Paul et al., 2014; Zhang et al., 2014; Aikman et al., 2012; Guo and Wilson, 2012; King et al., 2011). However, due to their large size, remoteness and high elevation, the following issues about Himalayan leucogranites still remain highly controversial: (1) most workers attributed the formation of Himalaya leucogranites to partial melting of the Higher Himalayan Sequence (HHS) (e.g., Gou et al., 2016; King et al., 2011; Zeng et al., 2011; Aoya et al., 2005; Booth et al., 2004; Guillot and Le Fort, 1995), whereas Guo and Wilson (2012) argued that the leucogranites were derived from both the Lesser Himalayan

Sequences (LHS) and the HHS (e.g., Guo and Wilson, 2012); (2) there is no suitable statement for the petrogenesis of the Himalayan leucogranites. Leucogranites are closely linked to either (a) vapour-absent anatexis (Patino Douce and Harris, 1998; Harris and Massey, 1994) or vapour-present melting (Gao and Zeng, 2014; Zeng et al., 2011; Clemens and Vielzeuf, 1987); or (b) decompression melting during exhumation (Hou et al., 2012; Harris and Massey, 1994) or prograde melting during continental subduction (Zhang et al., 2017; Gou et al., 2016; Sorcar et al., 2014; Groppo et al., 2012, 2010); or (c) radioactive heating melting associated with the radioactive elements (Searle and Szluc, 2005) or heating melting from the deeper thickened continental crust levels (Thompson and Connolly, 1995; Patino Douce et al., 1990) or frictional heating melting (Visonà and Lombardo, 2002); or (d) muscovite-dehydration melting (Imayama and Suzuki, 2013) or biotite-dehydration melting (Vielzeuf and Montel, 1994; Vielzeuf and Holloway, 1988); or (e) fractional crystallization (Wu et al., 2015; Liu et al., 2014; Wang et al., 2014; Scaillet et al., 1990); (3) the formation time of the Himalayan leucogranites were usually dated at 46–8 Ma, and whether these available U-(Th)-Pb ages should be interpreted as a long-lived and continued anatexis process (Zhang et al., 2017, 2015; Gou et al., 2016) or multiperiod magmatism is still highly controversial. Therefore, although many researches have focused on petrology and geochronology of the Himalayan leucogranites, their formation time and petrogenesis are still far from being universally demonstrated (Zhang et al., 2017).

*Corresponding author: dongxin5811935@163.com

© China University of Geosciences (Wuhan) and Springer-Verlag GmbH Germany, Part of Springer Nature 2019

Manuscript received November 25, 2018.

Manuscript accepted March 28, 2019.

In this paper, we report new geochemical and geochronological data for the Paiku leucogranites, northern Himalaya. These results, combined with antecedent researcches, are used to reveal the crystallization ages, petrogenesis and tectonic settings of the Himalayan leucogranites. Conceivably, our new results will provide new insights into the origin of Himalayan leucogranites and partial melting behavior of relatively deeper crustal rocks.

1 GEOLOGICAL BACKGROUND AND SAMPLES

The Himalaya Orogen, constructed through the convergence between the Indian and the Eurasian continents, is separated by the South Tibetan detachment (STD), the main central thrust (MCT) and the main boundary thrust (MBT), respectively, subdividing it into the Tethyan Himalayan Sequence (THS), the HHS, the LHS, and the Neogene Siwalik Formation (Yin, 2006; Fig. 1a).

Two belts of Oligocene–Miocene leucogranites intruded into the upper part of the HHS and THS, forming the Higher Himalayan leucogranites (HHL) to the south and Tethyan Himalayan leucogranites (THL) to the north (e.g., Guo and Wilson, 2012). The HHL occur as sheets, dykes, veins or rarely, stocks exposed adjacent to the STD, and the THL generally intruded into the core of the North Himalayan gneiss domes (Fig. 1a). The HHL are predominantly two-mica leucogranites, tourmaline leucogranites and garnet-bearing leucogranites, whereas the THL consists mainly of tourmaline leucogranite, garnet-bearing leucogranite, two-mica granite and cordierite-bearing leucogranite (Guo and Wilson, 2012; Guillot and Le Fort, 1995). Previous studies have indicated that the HHL crystallized at 37–10 Ma (Wu et al., 2015; Liu et al., 2014; Aikman

et al., 2012; Hou et al., 2012; King et al., 2011; Aoya et al., 2005), whereas the THL formed at 46–8 Ma (Gou et al., 2016; Guo and Wilson, 2012; Harrison et al., 1999).

The present study area is located at the northern Himalaya (Fig. 1a), and consists of Jurassic–Cretaceous pelitic and calcareous schist of the THS, mylonitic granites, leucogranites and Paiku Co (Fig. 1b). Presence of andalusite and skarn formation in the pelitic and calcareous schist indicates relatively intensive contact metamorphism in these sedimentary wall-rocks. Presence of mylonitic granites records multistage ductile deformation. The Paiku leucogranites, separated by Paiku Co, can be subdivided into (i) the TML, outcropping as a stock to the west, (ii) the GL, outcropping as a dyke to the west, (iii) the CL, outcropping as a batholith to the east, and (iv) the TL, outcropping as a dyke and veins to the west (Fig. 1b). Detailed field observations on the cross-cutting relationship of the four different rock types in Paiku Complex indicate that the TML occasionally intruded into the TL, and the TML, GL, CL, TL intruded into the mylonitic granites, showing no obvious contact relations among the TML, GL and CL.

Petrographic observations show that all four types of leucogranite are composed of quartz, plagioclase, K-feldspar and accessory minerals zircon, apatite and monazite. TMLs are always medium- to fine-grained rocks and consist of quartz, K-feldspar, plagioclase, and euhedral to subhedral muscovite and biotite (Fig. 2a). GLs are also usually medium- to coarse grained rocks, and contain up to 2%–5% large subhedral garnet and some fine-grained tourmaline (Fig. 2b); CLs typically consist of plagioclase, K-feldspar, quartz, muscovite, biotite, and cordierite (up to 3%–5%; Fig. 2c). TLs are usually medium- to coarse grained rocks, and have abundant (up to ~10%) large and euhedral to subhedral tourmaline grains with a compositionally zoned structure (Fig. 2d).

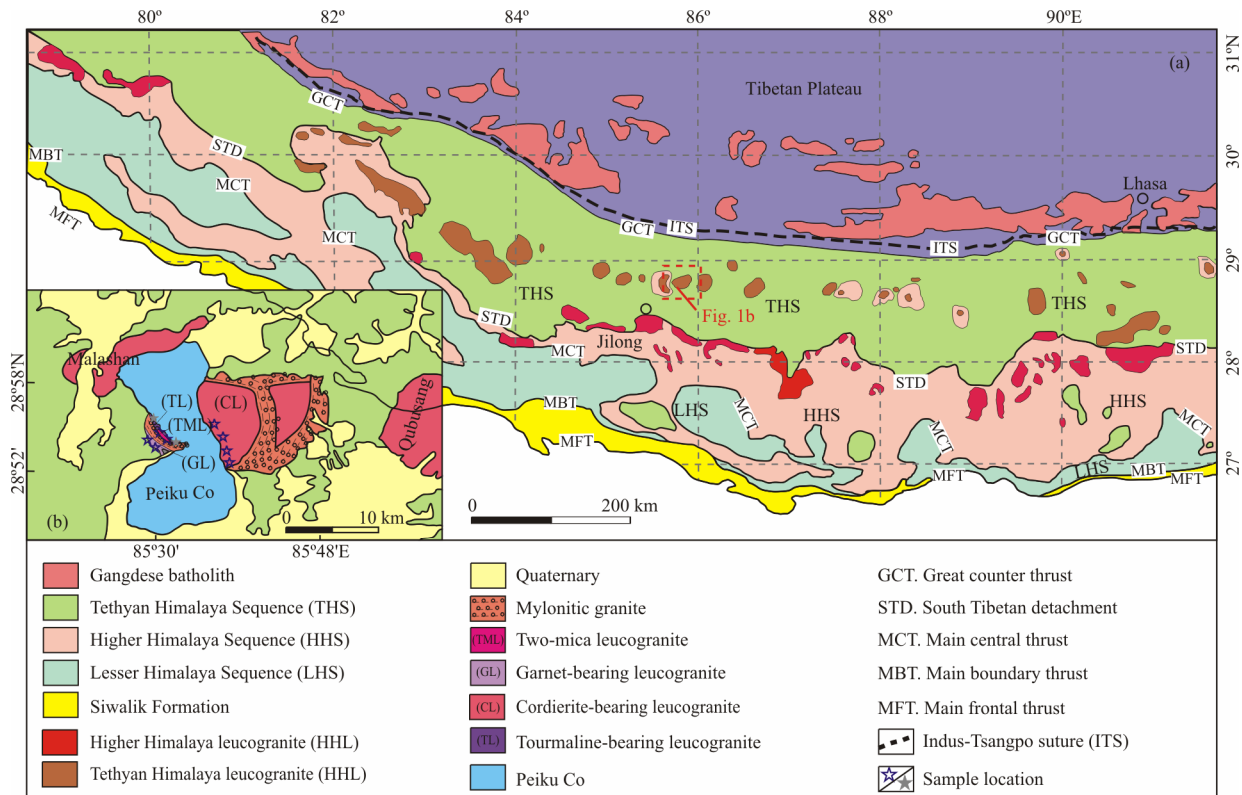


Figure 1. (a) Simplified geological map of northern Himalaya (modified after Guo and Wilson, 2012); (b) sketch geological map of the Paiku.

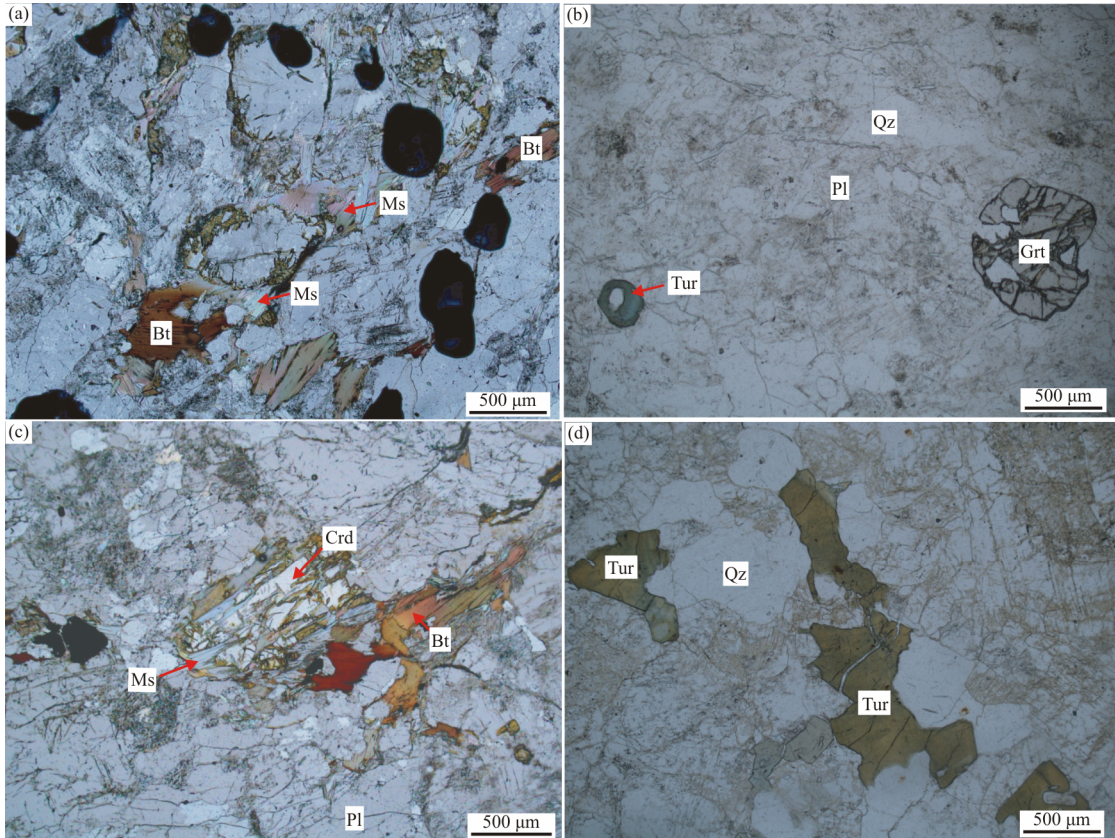


Figure 2. Photomicrographs of the Paiku leucogranites. (a) Two-mica leucogranite; (b) garnet-bearing leucogranite; (c) cordierite-bearing leucogranite; and (d) tourmaline-bearing leucogranite. Bt. Biotite; Ms. muscovite; Grt. garnet; Kf. K-feldspar; Pl. plagioclase; Qz. quartz; Tur. tourmaline.

2 ANALYTICAL METHODS

Whole-rock compositions were analyzed at the National Geological Analysis Center of China, Beijing. Oxides of major elements, including loss on ignition (LOI), were analyzed using X-ray fluorescence (XRF) (Rigaku-3080) with an analytical uncertainty of <0.5%. In order to obtain representative whole-rock compositions, approximately 1 kg of material was powdered. Trace elements Zr, Nb, V, Cr, Sr, Ba, Zn, Ni, Rb and Y were analyzed using a different XRF instrument (Rigaku-2100) with an analytical uncertainty of <3%–5%. Other trace elements and rare earth elements were analyzed using inductively coupled plasma mass spectrometry (ICP-MS, TJA-PQ-ExCell). Analytical uncertainties are 10% for elements with abundances <10 ppm, and around 5% for those >10 ppm. Cathodoluminescence imaging of zircon was performed using a HITACHI S2250-N scanning electron microscope at the SHRIMP unit at the Institute of Geology, Chinese Academy of Geological Sciences (CAGS), Beijing. Zircon U-Pb dating was carried out by LA-ICP-MS at the State Key Laboratory of Geological Processes and Mineral Resources, China University of Geosciences (Wuhan). Detailed operating conditions for the laser ablation system and the ICP-MS instrument are described by Liu et al. (2010). Laser sampling was performed using an Excimer 193 nm GeoLas 2005 System with a laser spot of 32 μm in diameter. An Agilent 7500a ICP-MS instrument was used to acquire ion-signal intensities. Zircon 91500 and the GSE-1 glass were used as an external standard for Pb/U ratio and concentration, respectively. Common Pb correction was made utilizing the

correction function (Andersen, 2002). Offline selection and integration of background and analyte signals, and time-drift correction and quantitative calibration were carried out using ICPMSDataCal (Liu et al., 2010). Concordia diagrams were made using ISOPLOT program (Ludwig, 2003).

3 RESULTS

3.1 Zircon U-Pb Ages

One TML (50-7), one GL (51-2) and two CLs (52-4 and 53-1) are selected for zircon U-Pb dating, and the results are shown in Figs. 3a–3d and listed in Table S1.

Zircon grains from one TML are colorless, transparent, and show euhedral prismatic in form (Fig. 3a). Cathodoluminescence images show that most of the zircon grains have core-rim structure. The inherited cores exhibit prismatic or irregular form, and show weak oscillatory zoning or no zoning. By contrast, the zircon rims display clear oscillatory zoning, typical of magmatic origin. To constrain more precisely on the crystallization ages of the Paiku leucogranites, U-Pb analysis were focused mainly on the oscillatory-zoned rims of zircon. Analyses on the TML obtain Th=133 ppm–3 597 ppm and U=917 ppm–9 256 ppm with relatively high Th/U ratios of 0.02–0.74 (Table S1), indicating magmatic origin (Hoskin and Schaltegger, 2003). The TML yields variable $^{206}\text{Pb}/^{238}\text{U}$ ages ranging from 23.1 to 17.2 Ma (Fig. 3a).

Zircon grains from the GL are colorless, and show euhedral to subhedral prismatic forms in cathodoluminescence images (Fig. 3b), zircon crystals exhibit mottled or spongy

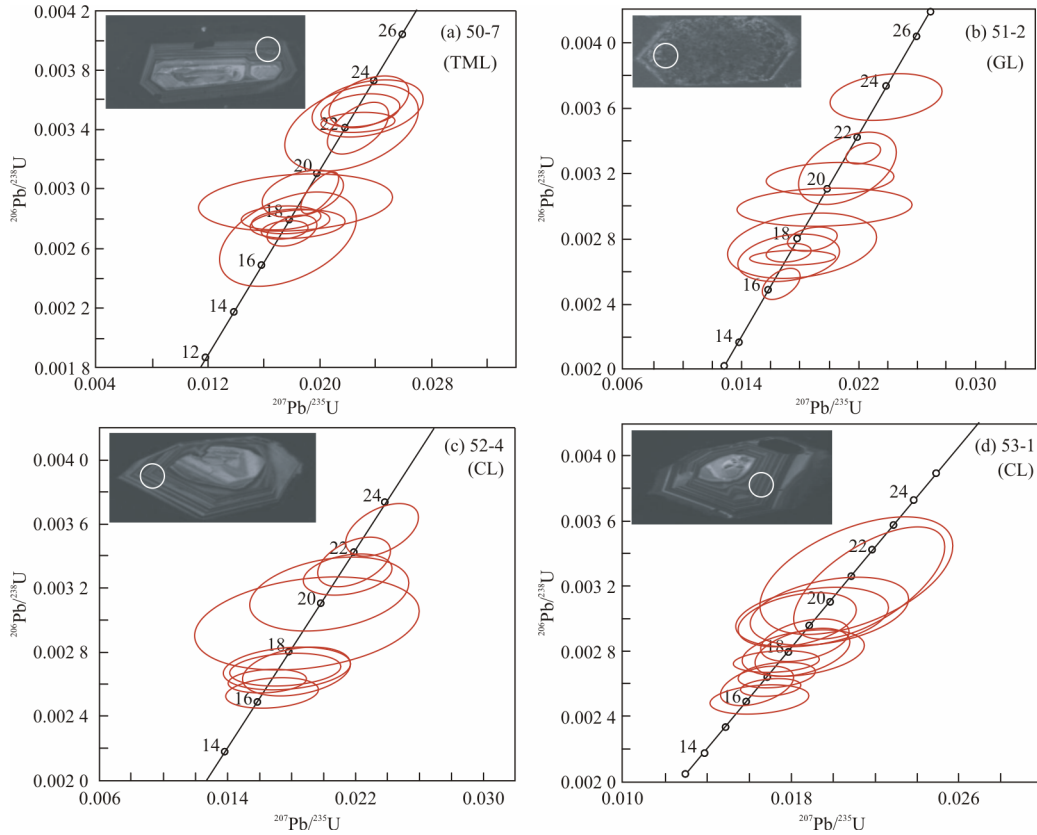


Figure 3. Zircon U-Pb concordia diagrams of representative zircons. The circles indicate the locations of U-Pb dating with a scale bar of 32 μm .

internal textures, which implies that the leucogranites had experienced different degrees of hydrothermal alteration process. Analyses on GL have Th=232 ppm–1 975 ppm and U=13 027 ppm–35 838 ppm with relatively low Th/U ratios of 0.01–0.07 (Table S1). The GL yields variable $^{206}\text{Pb}/^{238}\text{U}$ ages ranging from 23.6 to 16.3 Ma (Fig. 3b).

Most of the zircon grains in two CL samples show prismatic form, and have a similar core-rim structure (Figs. 3c and 3d). The inherited cores are either gray homogeneous or weak oscillatory growth zoning, and the zircon rims display clear oscillatory zoning. Analyses on the rims exhibit that they have a relatively wide range of Th and U concentrations from 88 ppm to 1 795 ppm, and from 3 643 ppm to 11 335 ppm, respectively, and Th/U from 0.02 to 0.30. The zircon rims yield $^{206}\text{Pb}/^{238}\text{U}$ ages from 22.9 to 16.4 Ma and 21.0 to 16.1 Ma (Figs. 3c and 3d).

As mentioned above, the magmatic zircon rims of the TML, GL, and CL yielded variable ages ranging from 23.6 to 16.1 Ma. Due to the well-developed oscillatory overgrowth zoning, we interpret these ages as the crystallization ages of the Paiku leucogranites.

3.2 Whole-Rock Major and Trace Elements

Whole-rock major and trace elements are listed in Table S2 and are shown graphically in Figs. 4–6. It is noted that major and trace elements of the TL are from Gao et al. (2013). Four types of Paiku leucogranites display different geochemical characteristics in major and trace elements. The TMLs have SiO_2 contents from 72.73 wt.% to 73.41 wt.%, K_2O contents of 3.92 wt.%–4.03 wt.%, Al_2O_3 varying from 14.98 wt.% to 15.11 wt.% (Figs. 4a, 4b, 5a, 5b; Table S2) and differentiation index (D.I.) of

89.06–89.23. The GLs have concentrated SiO_2 (74.68 wt.%–74.99 wt.%), Al_2O_3 (14.52 wt.%–14.74 wt.%) and K_2O (3.83 wt.%–4.08 wt.%) contents, and high Na_2O (4.28 wt.%–4.82 wt.%) and D.I. (93.90–94.12), but low CaO values (0.73 wt.%–0.80 wt.%). The CLs have SiO_2 of 71.84 wt.%–72.34 wt.%, Al_2O_3 of 14.87 wt.%–15.08 wt.%, total alkali ($\text{Na}_2\text{O}+\text{K}_2\text{O}$) of 7.24 wt.%–7.49 wt.%, CaO of 1.14 wt.%–1.34 wt.%, MgO of 0.63 wt.%–0.67 wt.% and D.I. of 85.56–86.76. The TLs have SiO_2 of 72.51 wt.%–72.54 wt.%, Al_2O_3 of 14.94 wt.%–14.95 wt.%, total alkali ($\text{Na}_2\text{O}+\text{K}_2\text{O}$) of 9.36 wt.%–9.43 wt.%, CaO of 0.70 wt.%–0.72 wt.%, MgO of 0.20 wt.%–0.22 wt.% and D.I. of 94.00–94.17. As compared to the GL and the TL, the TML and CL have higher Al_2O_3 (\geq 14.87 wt.%), TiO_2 (\geq 0.11 wt.%), MnO (\geq 0.02 wt.%), MgO (\geq 0.29 wt.%), CaO (\geq 1.14 wt.%), lower SiO_2 (\leq 73.41 wt.%), Na_2O (\leq 3.69 wt.%), total alkali ($\text{Na}_2\text{O}+\text{K}_2\text{O}$) (\leq 7.49 wt.%) and D.I. values (\leq 89.23) (Figs. 4a, 4b, 5a, 5b; Table S2). In general, the Paiku leucogranites are peraluminous and calc-alkalic to alkali-calcic rocks, characterized by high K_2O contents (\geq 3.66 wt.%) and A/CNK (\geq 1.08) (Fig. 4c). All the Paiku leucogranites are enriched in LREE, with moderately to strongly negative Eu anomalies ($\text{Eu}/\text{Eu}^*=0.12$ –0.71) (Fig. 6a; Table S2). On the primitive mantle-normalized trace elements diagram (Fig. 6b), the Paiku leucogranites show positive anomalies in Rb and Nb, but negative anomalies of Sr, Ba, K and Ti. Interestingly, these four types of Paiku leucogranites exhibit substantial differences in trace element compositions. GL and TL contain lower Sr (<39.7 ppm), Ba (<165 ppm), Th (<3.6 ppm), Zr (<33.5 ppm) and REE (<32.9 ppm) concentrations than TML and TL (Figs. 5d–5h). GL and CL are weakly depleted in HREE with $(\text{Gd}/\text{Yb})_{\text{N}}=0.10$ –0.27, whereas TML and TL are weakly enriched

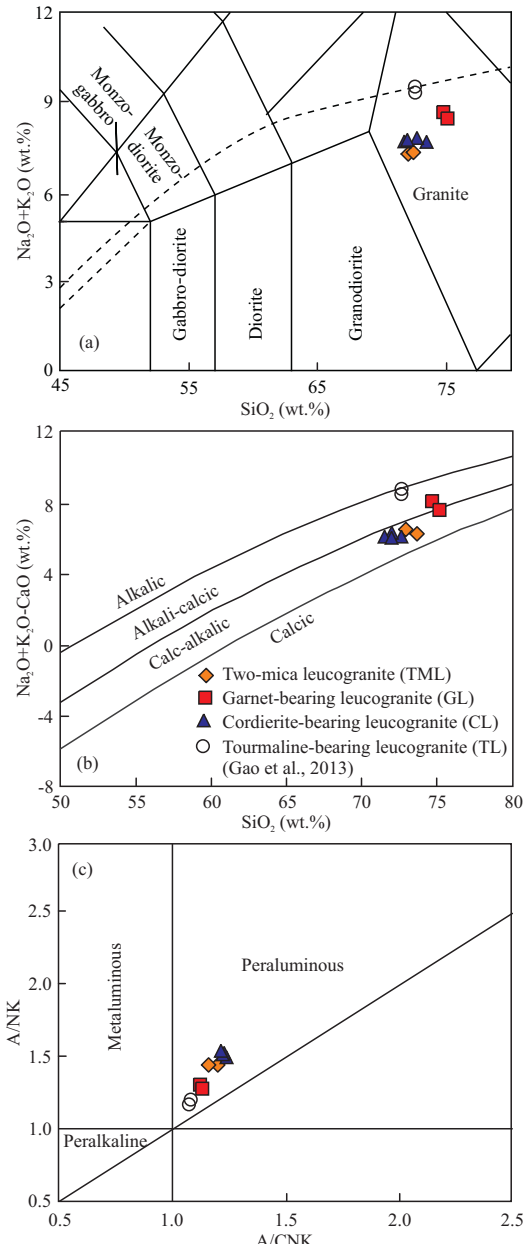


Figure 4. Variation diagrams of (a) $(\text{K}_2\text{O} + \text{Na}_2\text{O})$ vs. SiO_2 (Middlemost, 1994); (b) $(\text{Na}_2\text{O} + \text{K}_2\text{O} - \text{CaO})$ vs. SiO_2 (Frost et al., 2001), and (c) A/NK vs. A/CNK (Maniar and Piccoli, 1989).

in HREE with $(\text{Gd}/\text{Yb})_{\text{N}} = 0.15\text{--}0.30$ (Fig. 6a). And GL and CL show moderately positive P and Nb anomalies in contrast with negative anomalies in the TML and TL. Therefore, the present work indicates that different types of Paiku leucogranites show substantial differences in whole-rock major and trace elements.

4 DISCUSSION

4.1 Crystallization Ages of the Paiku Leucogranites

The Himalaya Orogen has experienced long-lived and continued metamorphism, deformation and partial melting, which is recorded by various types of leucogranites and migmatites (King et al., 2011; Zeng et al., 2011). U-Pb dating data of zircon and monazite from these Himalayan leucogranites indicate crystallization ages ranging from Eocene (Liu et al., 2014; Hou et al., 2012; Zeng et al., 2011) to Miocene (Searle and Godin, 2003; Harrison

et al., 1999; Edwards and Harrison, 1997; Schärer, 1984). Meanwhile, whether such a wide age span should be interpreted as a low degree of partial melting process (Zhang et al., 2017, 2015; Gou et al., 2016) or multi-stages magmatism is still controversial.

U-Pb geochronology suggests that the Paiku leucogranites have experienced a continued and low degree of partial melting process. The well-developed oscillatory-zoned zircon rims of one TML (50-7), one GL (51-2) and two CLs (52-4 and 53-1) yielded variable $^{206}\text{Pb}/^{238}\text{U}$ ages ranging of 23.1–17.2, 23.6–16.3, 22.9–16.4, and 21.0–16.1 Ma, respectively (Figs. 3a–3d), which represents the crystallization ages of the Paiku leucogranites, consistent with the ages reported by Wang et al. (2016), who revealed that the Paiku leucogranites have experienced at least two stages of anatexis. Gao et al. (2013) also concluded that the Paiku leucogranites have experienced multiple anatexis based on the crystallization ages of the TML and TL are 19.8 ± 0.5 and 28.2 ± 0.5 Ma.

It is well known that Himalayan leucogranites have scattered crystallization ages frequently. It was argued that such a wide age span may be due to analysis on zircon domains straddling cross different overgrowth zoning (Huang et al., 2017). However, the zircon age populations usually vary in a relatively large range of several Ma, even though we have carefully checked the U-Pb results and cathodoluminescence images, and make sure the obtained dating results are not the products of mixed ages. Fortunately, Rubatto et al. (2013) and Zhang et al. (2017) concluded that it is not surprising that zircon grains in Himalayan leucogranites frequently yield scattered and wide range of crystallization ages, based on the fact that melting and melt crystallization could occur over a long period of time when high temperatures were preserved, in that way new growth as well as dissolution and (re)precipitation of individual zircon grains could have occurred at any time. The crystallization ages of the Paiku leucogranites are 23.6–16.1 Ma, which are consistent with the 25–15 Ma time span proposed for the melt crystallization ages derived from the HHS (Fig. 3; Zhang et al., 2018b). Given the fact that the zircon U-Pb dating results can only represent the melt crystallization ages, rather than partial melting time, and the partial melting can occur 20 Ma earlier than melt crystallization, we propose that the Paiku leucogranites underwent a continued and low degree of partial melting process, rather than multi-stages magmatism.

4.2 Petrogenesis

Most studies have concluded that the source region of the Himalayan leucogranites are HHS (e.g., Zeng et al., 2014; King et al., 2011; Aoya et al., 2005), or two-component mixing between the LHS and the HHS (e.g., Guo and Wilson, 2012). Metapelites (Searle et al., 2009; Patino Douce and Harris, 1998; Guillot et al., 1995; Deniel et al., 1987), metagraywacke (Guillot and Le Fort, 1995), amphibolite (Gao et al., 2013; Zeng et al., 2011), felsic and pelitic HP granulites (Zhang et al., 2017) are potential source rocks for the HHL. We are more apt to the view that the Paiku leucogranites were derived from metasedimentary rocks of the HHS based on the following evidences: (1) the HHS, which mainly consists of pelitic schists and felsic gneisses, underwent coeval partial melting during the long-lived amphibolite to granulite facies metamorphism (Zhang et al., 2017; Sorcar et

al., 2014; Groppo et al., 2012). The phase equilibria modeling indicated that melt of 15%–20% may be produced for the HHS pelitic schists and felsic gneisses during their partial melting, and

more than half of the produced melt has escaped from its source and migrated (Zhang et al., 2017), the extracted voluminous melt can provide sufficient source for the formation of HHL. (2) Gao

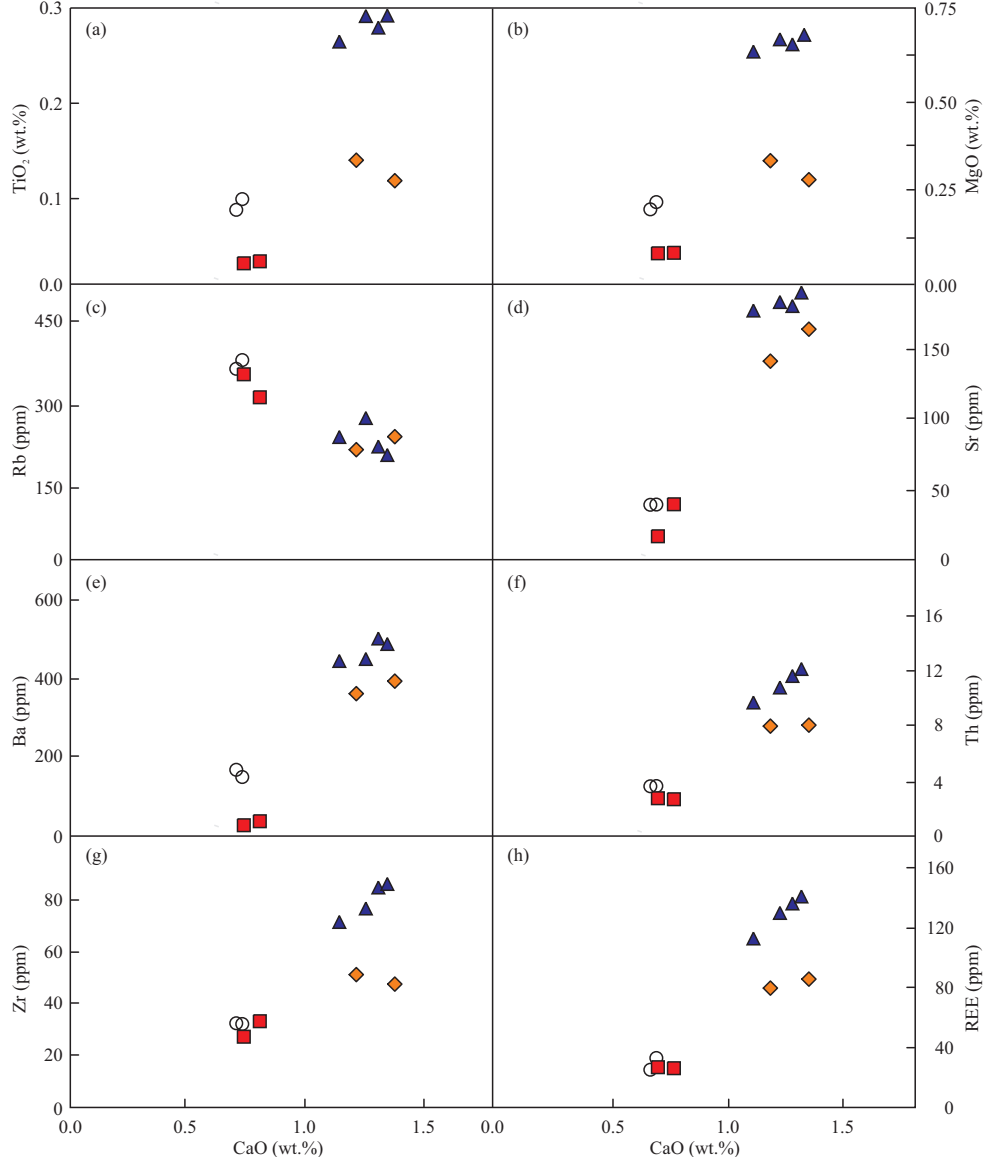


Figure 5. Harker plots of the Paiku leucogranites. The legend is the same as Fig. 4

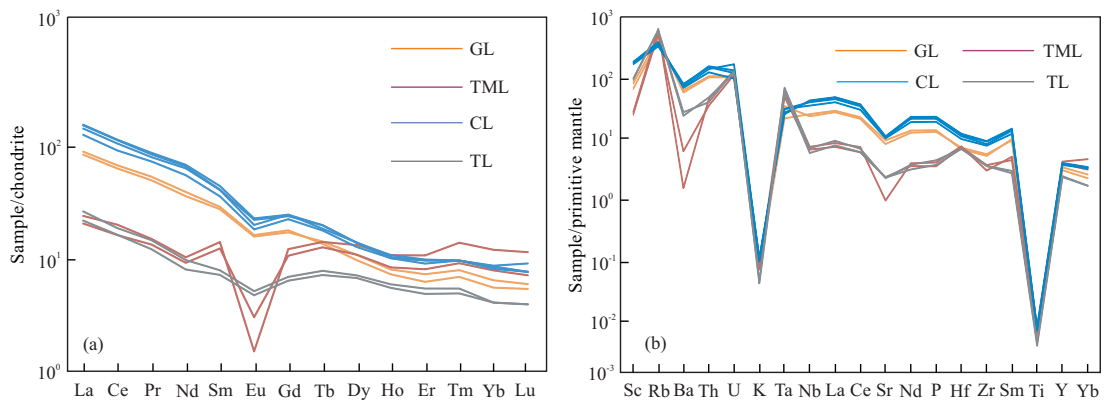


Figure 6. (a) Chondrite-normalized REE patterns and (b) primitive-mantle-normalized trace element patterns of the Paiku leucogranites. The normalization values are from Sun and McDonough (1989).

et al. (2013) suggested that the Paiku leucogranites have initial $^{87}\text{Sr}/^{86}\text{Sr}$ ratios from 0.728 5 to 0.752 5, unradiogenic initial Nd isotopic compositions ($\varepsilon_{\text{Hf}}(t)$) varying from -13.0 to -13.9. These characteristics imply that the Paiku leucogranites were derived from partial melting of HHS metapelite. Wang et al. (2016) revealed that the values of $(^{87}\text{Sr}/^{86}\text{Sr})$ of the Paiku granites range from 0.736 184 to 0.741 258, $\varepsilon_{\text{Hf}}(t)$ ranges from -14.6 to -14.3, and these characteristics can compare well with the metasedimentary rock in the HHS. (3) The Paiku leucogranites, characterized by high SiO_2 and Al_2O_3 concentrations and high A/CNK, are typical of S-type peraluminous granites. Besides, these leucogranites contain a mass of Al-rich minerals, such as tourmaline, muscovite, and cordierite, which suggests they were derived from metasedimentary rocks (Visonà and Lombardo, 2002).

Several mechanisms were proposed to explain the pronounced geochemical heterogeneity in major and trace elements as well as in isotope (e.g., Sr and Nd) geochemistry among different kinds of leucogranites, such as different source regimes (Visonà and Lombardo, 2002; Inger and Harris, 1993), different melting degrees or partial melting reactions (Gou et al., 2016; Patino Douce and Harris, 1998; Harris and Massey, 1994; Vielzeuf and Holloway, 1988), and fractional crystallization and assimilation (Wu et al., 2015; Liu et al., 2014; Wang et al., 2014; Scaillet et al., 1990). As discussed above, the TML, GL, CL and TL of the Paiku leucogranites exhibit similar initial $^{87}\text{Sr}/^{86}\text{Sr}$ ratios and small-span unradiogenic initial Nd isotopic compositions, which can rule out the possibility of different source regimes and assimilation models. The authors consider that the four types leucogranites in Paiku area were more likely derived from different partial melting reactions, rather than fractional crystallization, although the fractionation can not be completely excluded. The reasons are as follows: (1) Detailed field observations on the cross-cutting relationship of the Paiku leucogranites indicate that the TML occasionally intruded into the TL, which is not in agreement with crystallization hypothesis that the TL represents the evolved melt and therefore crystallized late. (2) The TML, GL and CL yielded similar zircon ages (23.6–16.1 Ma), and the TL, characterized by similar SiO_2 contents with the TML and CL, formed at 28.2 ± 0.5 Ma (Gao et al., 2013), these characteristics are inconsistent with the fractionation mechanism that decreasing zircon ages with increasing bulk SiO_2 concentrations of the four rock types. (3) Correlations of Al_2O_3 , CaO , MgO , TiO_2 and total alkali with SiO_2 are not obviously.

Most previous studies suggested that the HHLs were formed by muscovite-dehydration melting (Clemens and Stevens, 2015; Harris et al., 2004, 1993; Braun et al., 1996), or fluid-fluxed muscovite melting (Zeng et al., 2014, 2011; Gao et al., 2013). But we attribute the formation of the TML and CL in Paiku area to biotite-dehydration melting, whereas the GL and TL were mainly derived from the muscovite-dehydration melting of the HHS. The TML and CL were likely generated by the biotite-dehydration melting based on (1) low Rb/Sr ratios (1.01–1.86, avg. 1.30; Table S2) and high Sr (≥ 144.08 ppm) and Ba (≥ 365.52 ppm) contents of TML and CL indicate that these leucogranites were derived from biotite-dehydration melting (Icenhower and London, 1995); (2) as compared to the GL and TL, TML and CL display relatively high TiO_2 concentrations (0.11 wt.%–0.29 wt.%, avg. 0.23 wt.%; Table S2), which is consistent with fluid-absent biotite melting, because

biotite-dehydration melting could release Ti to the melt, and increase the Ti contents of the leucogranites obviously (avg. 0.17 wt.% about biotite-dehydration melting) (Huang et al., 2017; Liu et al., 2014; King et al., 2011); (3) compared with the GL and TL, the TML and CL are characterized by higher MgO , Ti, Ba, Sr and LREE concentrations (Table S2), indicating significant amounts of biotite were involved during the partial melting of the HHS (Liu et al., 2014; Visonà and Lombardo, 2002). (4) TML and CL have higher melt temperatures than GL and TL (Table S2), and such high melt temperatures are sufficient to induce biotite-dehydration melting of the HHS (e.g., Zhang et al., 2018b, 2017; Gou et al., 2016; Sorcar et al., 2014; Groppo et al., 2012).

We consider that the GL and TL were mainly derived from the muscovite-dehydration melting of the metasedimentary rocks of the HHS based on (1) high Rb/Sr ratios (8.07–24; Table S2) and low Sr (<39.76 ppm) and Ba (<165 ppm) contents of the GL and TL are the typical representative of muscovite-dehydration melting (Harrison et al., 1999); (2) the Rb/Sr ratios of the GL and TL are negatively correlated with Ba concentrations (Fig. 7), which are consistent with muscovite-dehydration melting (Harris and Inger, 1992); (3) the GL and TL have relatively low TiO_2 concentrations (0.02 wt.%–0.09 wt.%, avg. 0.05 wt.%; Table S2), Eu/Eu* ratios (avg. 0.45), Ce/Ce* ratios (avg. 0.75), Ba (avg. 88.5 ppm), Sr (avg. 33.2 ppm), Th (avg. 3.1 ppm), Zr (avg. 31.3 ppm), LREE (avg. 19.34 ppm), and Hf (avg. 1.77 ppm) contents, which are distinctive features of fluid-absent dehydration melting of muscovite (Table S2; Patino Douce and Harris, 1998; Inger and Harris, 1993; Harris and Inger, 1992).

4.3 Tectonic Implications

Most previous studies proposed that the Himalayan leucogranites were generated in extension-related tectonic setting based on their Oligocene–Miocene crystallization ages and the relationship with the STD (e.g., Guo and Wilson, 2012; Zhang et al., 2004; Harris and Massey, 1994; Burchfiel and Royden, 1985). However, some recent studies argued that the Himalayan leucogranites could be formed in a contractive tectonic setting (Zhang et al., 2018a; Liu et al., 2014; Zeng et al., 2014; Gao et al., 2011; Ding et al., 2005; Visonà and Lombardo, 2002).

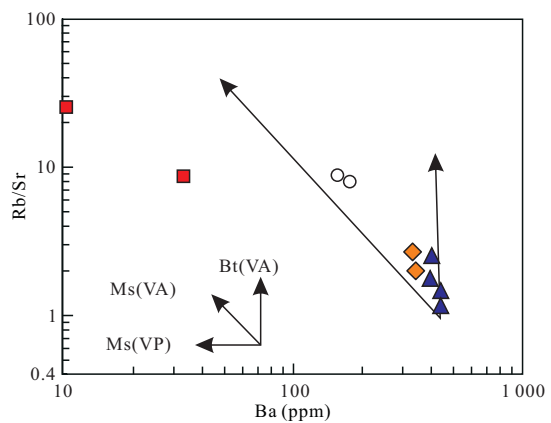


Figure 7. Diagram of Rb/Sr ratios vs. Ba. Ms(VP), Ms(VA) and Bt(VA) represent trends of vapor-present muscovite melting, vapor-absent muscovite and biotite melting, respectively (Inger and Harris, 1993). The legend is the same as Fig. 4

Recent phase equilibria modeling studies have demonstrated that the partial melting of the HHS occurred dominantly during the prograde and peak metamorphism (e.g., Zhang et al., 2015; Sorcar et al., 2014; Rubatto et al., 2013; Groppo et al., 2012, 2010; Guilmette et al., 2011). It indicates that the anatexis of the HHS occurred at a contractive tectonic setting.

Our previous results (Zhang et al., 2018b; Gou et al., 2016) showed that pelitic and felsic rocks from the HHS underwent a long lasting granulite-facies metamorphism, partial melting and melt crystallization process which began at ca. 40 Ma, and lasted to ca. 7 Ma (Fig. 11 in Gou et al., 2016; Fig. 3 in Zhang et al., 2018b and references therein). The partial melting of the HHS occurred firstly by the muscovite-dehydration melting and followed by the biotite-dehydration melting during prograde and peak metamorphism, which resulted in formation of melts with highly variable chemical compositions. Moreover, the generated melts, produced by dehydration melting of both muscovite and biotite, could crystallize among the whole processes, so it is not surprising that the Himalayan leucogranites have scattered crystallization ages. Recent works (Zhang et al., 2017; Gou et al., 2016; Rubatto et al., 2013) confirmed that granulite-facies metamorphism and anatexis of the HHS occurred as early as 45 Ma, and lasted to 15 Ma. Besides, earlier emplacement of leucogranites at 43–32 Ma was also reported (e.g., Hou et al., 2012; Zeng et al., 2011). These results demonstrate that the anatexis of the HHS was earlier than the initial active time of the MCT and STD (~25 Ma), and it indicates further that the Himalayan leucogranites are not a consequence of decompression melting linked to exhumation of the HHS along the MCT and STD. Therefore, combining with previous results, we propose that the Paiku leucogranites were probably formed during the subduction of the Indian crust.

5 CONCLUSIONS

(1) The Paiku leucogranites are high-K, peraluminous rocks, and could be subdivided into TML, GL, CL and TL four types.

(2) The Paiku leucogranites were derived from metasedimentary rocks of the HHS, GL and TL were mainly resulted from fluid-absent muscovite-dehydration melting of the HHS; whereas the TML and CL were mainly derived from the biotite-dehydration melting.

(3) The Paiku leucogranites experienced a low degree of partial melting process, and were probably formed during the subduction of the Indian crust.

ACKNOWLEDGMENTS

This study was supported by the National Natural Science Foundation of China (Nos. 41872070, 41802071, 41773026 and 41303028), and the China Geological Survey (No. DD20190053). We thank Zuolin Tian, Wangchao Li and Lei Tang for sample collecting. We thank two anonymous reviewers for constructive and critical reviews that helped to improve the manuscript significantly. The final publication is available at Springer via <https://doi.org/10.1007/s12583-019-1219-8>.

Electronic Supplementary Materials: Supplementary materials (Tables S1–S2) are available in the online version of this article at <https://doi.org/10.1007/s12583-019-1219-8>.

REFERENCES CITED

- Andersen, T., 2002. Correction of Common Lead in U-Pb Analyses that do not Report ^{204}Pb . *Chemical Geology*, 192(1/2): 59–79. [https://doi.org/10.1016/s0009-2541\(02\)00195-x](https://doi.org/10.1016/s0009-2541(02)00195-x)
- Aikman, A. B., Harrison, T. M., Hermann, J., 2012. Age and Thermal History of Eo- and Neohimalayan Granitoids, Eastern Himalaya. *Journal of Asian Earth Sciences*, 51: 85–97. <https://doi.org/10.1016/j.jseas.2012.01.011>
- Aoya, M., Wallis, S. R., Terada, K., et al., 2005. North-South Extension in the Tibetan Crust Triggered by Granite Emplacement. *Geology*, 33(11): 853–856. <https://doi.org/10.1130/g21806.1>
- Booth, A. L., Zeitler, P., Kidd, W., et al., 2004. U-Pb Zircon Constraints on the Tectonic Evolution of Southeastern Tibet, Namche Barwa Area. *American Journal of Science*, 304(10): 889–929. <https://doi.org/10.2475/ajs.304.10.889>
- Braun, I., Raith, M., Kumar, G. R. R., 1996. Dehydration-Melting Phenomena in Leptynitic Gneisses and the Generation of Leucogranites: A Case Study from the Kerala Khondalite Belt, Southern India. *Journal of Petrology*, 37(6): 1285–1305. <https://doi.org/10.1093/petrology/37.6.1285>
- Burchfiel, B. C., Royden, L. H., 1985. North-South Extension within the Convergent Himalayan Region. *Geology*, 13(10): 679–682. [https://doi.org/10.1130/0091-7613\(1985\)13<679:newtch>2.0.co;2](https://doi.org/10.1130/0091-7613(1985)13<679:newtch>2.0.co;2)
- Clemens, J. D., Vielzeuf, D., 1987. Constraints on Melting and Magma Production in the Crust. *Earth and Planetary Science Letters*, 86(2/3/4): 287–306. [https://doi.org/10.1016/0012-821x\(87\)90227-5](https://doi.org/10.1016/0012-821x(87)90227-5)
- Clemens, J. D., Stevens, G., 2015. Comment on ‘Water-Fluxed Melting of the Continental Crust: A Review’ by R. F. Weinberg and P. Hasalová. *Lithos*, 234/235: 100–101. <https://doi.org/10.1016/j.lithos.2015.06.032>
- Deniel, C., Vidal, P., Fernandez, A., et al., 1987. Isotopic Study of the Manaslu Granite (Himalaya, Nepal): Inferences on the Age and Source of Himalayan Leucogranites. *Contributions to Mineralogy and Petrology*, 96(1): 78–92. <https://doi.org/10.1007/bf00375529>
- Ding, L., Kapp, P., Wan, X. Q., 2005. Paleocene–Eocene Record of Ophiolite Obduction and Initial India-Asia Collision, South Central Tibet. *Tectonics*, 24(3): 1–18. <https://doi.org/10.1029/2004tc001729>
- Edwards, M. A., Harrison, T. M., 1997. When did the Roof Collapse? Late Miocene North-South Extension in the High Himalaya Revealed by Th-Pb Monazite Dating of the Khula Kangri Granite. *Geology*, 25(6): 543–546. [https://doi.org/10.1130/0091-7613\(1997\)025<0543:wdtrcl>2.3.co;2](https://doi.org/10.1130/0091-7613(1997)025<0543:wdtrcl>2.3.co;2)
- Frost, B. R., Barnes, C. G., Collins, W. J., et al., 2001. A Geochemical Classification for Granitic Rocks. *Journal of Petrology*, 42(11): 2033–2048. <https://doi.org/10.1093/petrology/42.11.2033>
- Gao, L. E., Zeng, L. S., 2014. Fluxed Melting of Metapelite and the Formation of Miocene High-CaO Two-Mica Granites in the Malashan Gneiss Dome, Southern Tibet. *Geochimica et Cosmochimica Acta*, 130: 136–155. <https://doi.org/10.1016/j.gca.2014.01.003>
- Gao, L. E., Zeng, L. S., Hou, K. J., et al., 2013. Episodic Crustal Anatexis and the Formation of Paiku Composite Leucogranitic Pluton in the Malashan Gneiss Dome, Southern Tibet. *Chinese Science Bulletin*, 58(28/29): 3546–3563. <https://doi.org/10.1007/s11434-013-5792-4>
- Gao, L. E., Zeng, L. S., Xie, K. J., 2011. Eocene High Grade Metamorphism and Crustal Anatexis in the North Himalaya Gneiss Domes, Southern Tibet. *Chinese Science Bulletin*, 57(36): 3078–3090 (in Chinese)
- Gou, Z. B., Zhang, Z. M., Dong, X., et al., 2016. Petrogenesis and Tectonic Implications of the Yadong Leucogranites, Southern Himalaya. *Lithos*, 256/257: 300–310. <https://doi.org/10.1016/j.lithos.2016.04.009>
- Groppi, C., Rubatto, D., Rolfo, F., et al., 2010. Early Oligocene Partial Melting in the Main Central Thrust Zone (Arun Valley, Eastern Nepal Himalaya). *Lithos*, 118(3/4): 287–301. <https://doi.org/10.1016/j.lithos.2010.05.003>
- Groppi, C., Rolfo, F., Indares, A., 2012. Partial Melting in the Higher

- Himalayan Crystallines of Eastern Nepal: The Effect of Decompression and Implications for the ‘Channel Flow’ Model. *Journal of Petrology*, 53(5): 1057–1088. <https://doi.org/10.1093/petrology/egs009>
- Guillot, S., Le Fort, P., Pécher, A., et al., 1995. Contact Metamorphism and Depth of Emplacement of the Manaslu Granite (Central Nepal). Implications for Himalayan Orogenesis. *Tectonophysics*, 241(1/2): 99–119. [https://doi.org/10.1016/0040-1951\(94\)00144-x](https://doi.org/10.1016/0040-1951(94)00144-x)
- Guillot, S., Le Fort, P., 1995. Geochemical Constraints on the Bimodal Origin of High Himalayan Leucogranites. *Lithos*, 35(3/4): 221–234. [https://doi.org/10.1016/0024-4937\(94\)00052-4](https://doi.org/10.1016/0024-4937(94)00052-4)
- Guilmette, C., Indares, A., Hébert, R., 2011. High-Pressure Anatetic Paragneisses from the Namche Barwa, Eastern Himalayan Syntaxis: Textural Evidence for Partial Melting, Phase Equilibria Modeling and Tectonic Implications. *Lithos*, 124(1/2): 66–81. <https://doi.org/10.1016/j.lithos.2010.09.003>
- Guo, Z. F., Wilson, M., 2012. The Himalayan Leucogranites: Constraints on the Nature of Their Crustal Source Region and Geodynamic Setting. *Gondwana Research*, 22(2): 360–376. <https://doi.org/10.1016/j.gr.2011.07.027>
- Harris, N., Inger, S., 1992. Trace Element Modelling of Pelite-Derived Granites. *Contributions to Mineralogy and Petrology*, 110(1): 46–56. <https://doi.org/10.1007/bf00310881>
- Harris, N., Massey, J., Inger, S., 1993. The Role of Fluids in the Formation of High Himalayan Leucogranites. *Geological Society, London, Special Publications*, 74(1): 391–400. <https://doi.org/10.1144/gsl.sp.1993.074.01.26>
- Harris, N., Massey, J., 1994. Decompression and Anatexis of Himalayan Metapelites. *Tectonics*, 13(6): 1537–1546. <https://doi.org/10.1029/94tc01611>
- Harris, N., Caddick, M., Kosler, J., et al., 2004. The Pressure-Temperature-Time Path of Migmatites from the Sikkim Himalaya. *Journal of Metamorphic Geology*, 22(3): 249–264. <https://doi.org/10.1111/j.1525-1314.2004.00511.x>
- Harrison, M. T., Grove, M., McKeegan, K. D., et al., 1999. Origin and Episodic Emplacement of the Manaslu Intrusive Complex, Central Himalaya. *Journal of Petrology*, 40(1): 3–19. <https://doi.org/10.1093/petro/40.1.3>
- Hoskin, P. W. O., Schaltegger, U., 2003. The Composition of Zircon and Igneous and Metamorphic Petrogenesis. *Reviews in Mineralogy and Geochemistry*, 53(1): 27–62. <https://doi.org/10.2113/0530027>
- Hou, Z. Q., Zheng, Y. C., Zeng, L. S., et al., 2012. Eocene-Oligocene Granitoids in Southern Tibet: Constraints on Crustal Anatexis and Tectonic Evolution of the Himalayan Orogen. *Earth and Planetary Science Letters*, 349/350: 38–52. <https://doi.org/10.1016/j.epsl.2012.06.030>
- Huang, C. M., Zhao, Z. D., Li, G. M., et al., 2017. Leucogranites in Lhazag, Southern Tibet: Implications for the Tectonic Evolution of the Eastern Himalaya. *Lithos*, 294/295: 246–262. <https://doi.org/10.1016/j.lithos.2017.09.014>
- Icenhower, J., London, D., 1995. An Experimental Study of Element Partitioning among Biotite, Muscovite, and Coexisting Peraluminous Silicic Melt at 200 MPa (H_2O). *American Mineralogist*, 80(11/12): 1229–1251. <https://doi.org/10.2138/am-1995-11-1213>
- Imayama, T., Suzuki, K., 2013. Carboniferous Inherited Grain and Age Zoning of Monazite and Xenotime from Leucogranites in Far-Eastern Nepal: Constraints from Electron Probe Microanalysis. *American Mineralogist*, 98(8/9): 1393–1406. <https://doi.org/10.2138/am.2013.4267>
- Inger, S., Harris, N., 1993. Geochemical Constraints on Leucogranite Magmatism in the Langtang Valley, Nepal Himalaya. *Journal of Petrology*, 34(2): 345–368. <https://doi.org/10.1093/petrology/34.2.345>
- King, J., Harris, N., Argles, T., et al., 2011. Contribution of Crustal Anatexis to the Tectonic Evolution of Indian Crust beneath Southern Tibet. *Geological Society of America Bulletin*, 123(1/2): 218–239. <https://doi.org/10.1130/b30085.1>
- Liu, Y. S., Hu, Z. C., Zong, K. Q., et al., 2010. Reappraisal and Refinement of Zircon U-Pb Isotope and Trace Element Analyses by LA-ICP-MS. *Chinese Science Bulletin*, 55(15): 1535–1546. <https://doi.org/10.1007/s11434-010-3052-4>
- Liu, Z. C., Wu, F. Y., Ji, W. Q., et al., 2014. Petrogenesis of the Ramba Leucogranite in the Tethyan Himalaya and Constraints on the Channel Flow Model. *Lithos*, 208/209: 118–136. <https://doi.org/10.1016/j.lithos.2014.08.022>
- Ludwig, K. R., 2003. Isoplot/Ex Version 3.00: A Geochronological Toolkit for Microsoft Excel. Berkeley Geochronology Center, Special Publication, Berkeley. 1–73
- Maniar, P. D., Piccoli, P. M., 1989. Tectonic Discrimination of Granitoids. *Geological Society of America Bulletin*, 101(5): 635–643. [https://doi.org/10.1130/0016-7606\(1989\)101<0635:tdog>2.3.co;2](https://doi.org/10.1130/0016-7606(1989)101<0635:tdog>2.3.co;2)
- Middlemost, E. A. K., 1994. Naming Materials in the Magma/Igneous Rock System. *Earth-Science Reviews*, 37(3/4): 215–224. [https://doi.org/10.1016/0012-8252\(94\)90029-9](https://doi.org/10.1016/0012-8252(94)90029-9)
- Patino Douce, A. E., Harris, N., 1998. Experimental Constraints on Himalayan Anatexis. *Journal of Petrology*, 39(4): 689–710. <https://doi.org/10.1093/petro/39.4.689>
- Patino Douce, A. E., Humphreys, E. D., Johnston, A. D., 1990. Anatexis and Metamorphism in Tectonically Thickened Continental Crust Exemplified by the Sevier Hinterland, Western North America. *Earth and Planetary Science Letters*, 97(3/4): 290–315. [https://doi.org/10.1016/0012-821x\(90\)90048-3](https://doi.org/10.1016/0012-821x(90)90048-3)
- Paul, A., Jung, S., Romer, R. L., et al., 2014. Petrogenesis of Synorogenic High-Temperature Leucogranites (Damaran Orogen, Namibia): Constraints from U-Pb Monazite Ages and Nd, Sr and Pb Isotopes. *Gondwana Research*, 25(4): 1614–1626. <https://doi.org/10.1016/j.gr.2013.06.008>
- Rubatto, D., Chakraborty, S., Dasgupta, S., 2013. Timescales of Crustal Melting in the Higher Himalayan Crystallines (Sikkim, Eastern Himalaya) Inferred from Trace Element-Constrained Monazite and Zircon Chronology. *Contributions to Mineralogy and Petrology*, 165(2): 349–372. <https://doi.org/10.1007/s00410-012-0812-y>
- Scaillet, B., France-Lanord, C., Le Fort, P., 1990. Badrinath-Gangotri Plutons (Garhwal, India): Petrological and Geochemical Evidence for Fractionation Processes in a High Himalayan Leucogranite. *Journal of Volcanology and Geothermal Research*, 44(1/2): 163–188. [https://doi.org/10.1016/0377-0273\(90\)90017-a](https://doi.org/10.1016/0377-0273(90)90017-a)
- Schärer, U., 1984. The Effect of Initial ^{230}Th Disequilibrium on Young U-Pb Ages: The Makalu Case, Himalaya. *Earth and Planetary Science Letters*, 67(2): 191–204. [https://doi.org/10.1016/0012-821x\(84\)90114-6](https://doi.org/10.1016/0012-821x(84)90114-6)
- Searle, M. P., Godin, L., 2003. The South Tibetan Detachment and the Manaslu Leucogranite: A Structural Reinterpretation and Restoration of the Annapurna-Manaslu Himalaya, Nepal. *The Journal of Geology*, 111(5): 505–523. <https://doi.org/10.1086/376763>
- Searle, M. P., Szulc, A. G., 2005. Channel Flow and Ductile Extrusion of the High Himalayan Slab—The Kangchenjunga-Darjeeling Profile, Sikkim Himalaya. *Journal of Asian Earth Sciences*, 25(1): 173–185. <https://doi.org/10.1016/j.jseas.2004.03.004>
- Searle, M. P., Cottle, J. M., Streule, M. J., et al., 2009. Crustal Melt Granites and Migmatites along the Himalaya: Melt Source, Segregation, Transport and Granite Emplacement Mechanisms. *Earth and Environmental Science Transactions of the Royal Society of Edinburgh*, 100(1/2): 219–233. <https://doi.org/10.1017/s175569100901617x>
- Sorcar, N., Hoppe, U., Dasgupta, S., et al., 2014. High-Temperature Cooling Histories of Migmatites from the High Himalayan Crystallines in Sikkim, India: Rapid Cooling Unrelated to Exhumation?. *Contributions to Mineralogy and Petrology*, 167(2): 1–34. <https://doi.org/10.1007/s00410-013-0957-3>
- Sun, S. S., McDonough, W. F., 1989. Chemical and Isotopic Systematics of

- Oceanic Basalts: Implications for Mantle Composition and Processes. *Geological Society, London, Special Publications*, 42(1): 313–345. <https://doi.org/10.1144/gsl.sp.1989.042.01.19>
- Thompson, A. B., Connolly, J. A. D., 1995. Melting of the Continental Crust: Some Thermal and Petrological Constraints on Anatexis in Continental Collision Zones and other Tectonic Settings. *Journal of Geophysical Research: Solid Earth*, 100(B8): 15565–15579. <https://doi.org/10.1029/95jb00191>
- Vielzeuf, D., Holloway, J. R., 1988. Experimental Determination of the Fluid-Absent Melting Relations in the Pelitic System. *Contributions to Mineralogy and Petrology*, 98(3): 257–276. <https://doi.org/10.1007/bf00375178>
- Vielzeuf, D., Montel, J. M., 1994. Partial Melting of Metagreywackes. Part I. Fluid-Absent Experiments and Phase Relationships. *Contributions to Mineralogy and Petrology*, 117(4): 375–393. <https://doi.org/10.1007/bf00307272>
- Visonà, D., Lombardo, B., 2002. Two-Mica and Tourmaline Leucogranites from the Everest-Makalu Region (Nepal-Tibet). Himalayan Leucogranite Genesis by Isobaric Heating?. *Lithos*, 62(3/4): 125–150. [https://doi.org/10.1016/s0024-4937\(02\)00112-3](https://doi.org/10.1016/s0024-4937(02)00112-3)
- Wang, L. X., Ma, C. Q., Zhang, C., et al., 2014. Genesis of Leucogranite by Prolonged Fractional Crystallization: A Case Study of the Mufushan Complex, South China. *Lithos*, 206/207: 147–163. <https://doi.org/10.1016/j.lithos.2014.07.026>
- Wang, X. X., Zhang, J. J., Wang, J. M., 2016. Geochronology and Formation Mechanism of the Paiku Granite in Northern Himalaya, and Its Tectonic Implications. *Earth Science*, 41: 982–998 (in Chinese with English Abstract)
- Wu, F. Y., Liu, Z. C., Liu, X. C., et al. 2015. Himalayan Leucogranites: Petrogenesis and Implications to Orogenesis and Plateau Uplift. *Acta Petrologica Sinica*, 31: 1–36 (in Chinese with English Abstract)
- Yin, A., 2006. Cenozoic Tectonic Evolution of the Himalayan Orogen as Constrained by Along-Strike Variation of Structural Geometry, Exhumation History, and Foreland Sedimentation. *Earth-Science Reviews*, 76(1/2): 1–131. <https://doi.org/10.1016/j.earscirev.2005.05.004>
- Zeng, L. S., Gao, L. E., Xie, K. J., et al., 2011. Mid-Eocene High Sr/Y Granites in the Northern Himalayan Gneiss Domes: Melting Thickened Lower Continental Crust. *Earth and Planetary Science Letters*, 303(3/4): 251–266. <https://doi.org/10.1016/j.epsl.2011.01.005>
- Zeng, L. S., Gao, L. E., Tang, S. H., et al., 2014. Eocene Magmatism in the Tethyan Himalaya, Southern Tibet. *Geological Society, London, Special Publications*, 412(1): 287–316. <https://doi.org/10.1144/sp412.8>
- Zhang, H. F., Harris, N., Parrish, R., et al., 2004. U-Pb Ages of Kude and Sajia Leucogranites in Sajia Dome from North Himalaya and Their Geological Implications. *Chinese Science Bulletin*, 49(19): 2087. <https://doi.org/10.1360/04wd0198>
- Zhang, Z. M., Dong, X., Santosh, M., et al., 2014. Metamorphism and Tectonic Evolution of the Lhasa Terrane, Central Tibet. *Gondwana Research*, 25(1): 170–189. <https://doi.org/10.1016/j.gr.2012.08.024>
- Zhang, Z. M., Xiang, H., Dong, X., et al., 2015. Long-Lived High-Temperature Granulite-Facies Metamorphism in the Eastern Himalayan Orogen, South Tibet. *Lithos*, 212–215: 1–15. <https://doi.org/10.1016/j.lithos.2014.10.009>
- Zhang, Z. M., Xiang, H., Dong, X., et al., 2017. Oligocene HP Metamorphism and Anatexis of the Higher Himalayan Crystalline Sequence in Yadong Region, East-Central Himalaya. *Gondwana Research*, 41: 173–187. <https://doi.org/10.1016/j.gr.2015.03.002>
- Zhang, Z. M., Kang, D. Y., Ding, H. X., et al., 2018a. Partial Melting of Himalayan Orogen and Formation Mechanism of Leucogranites. *Earth Science*, 43(1): 82–98 (in Chinese with English Abstract)
- Zhang, Z. M., Ding, H. X., Dong, X., et al., 2018b. High-Temperature Metamorphism, Anatexis and Tectonic Evolution of a Mafic Granulite from the Eastern Himalayan Orogen. *Journal of Earth Science*, 29(5): 1010–1025. <https://doi.org/10.1007/s12583-018-0852-y>